Environ Geochem Health (2023) 45:7033–7050
https://doi.org/10.1007/s10653-023-01621-9

ORIGINAL PAPER

Natural carbon mineralization and its control on the geochemical evolution of coal-based aquifers in the Salt Range, Punjab, Pakistan

Noshin Masood · Karen A. Hudson-Edwards · Tehseen Zafar · Abida Farooqi

Received: 15 February 2023 / Accepted: 14 May 2023 / Published online: 31 May 2023

Abstract Hydrochemical analysis of the Salt Range was conducted to understand carbon weathering and its impact on groundwater evolution within the complex geological framework of Punjab. Our results showed that groundwater samples were alkaline with a pH range of 7.0–8.6 and 7.8–8.8 for the eastern Salt Range (ESR) and Trans-Indus Salt Range (TSR), respectively, while that of the Central Salt Range (CSR) was acidic to moderately alkaline ranging between 5.7 and 7.5. The water types of Ca-Mg-HCO_3, Ca–Mg–Cl, and Ca–Cl_2 were the dominant hydro-chemical facies in ESR and CSR sites. However, groundwater of the TSR site falls under Ca–Mg–Cl, Ca–Cl_2, and mixed types of Ca–Mg–SO_4. Our new findings suggest that groundwater chemistry is primarily controlled by rock dominance and reverse ion exchange reaction, followed by evapotranspiration processes. The wells of ESR, CSR, and TSR were reported with higher levels of Fe and Zn. Regarding the suitability for irrigation, sodium adsorption ratio (SAR), magnesium adsorption ratio (MAR), sodium percentage (Na%), Kelley's ratio (KR), and potential salinity (PS) at all three sites (ESR, TSR, and CSR) had the potential to become a salinity hazard. The conceptual model of geochemical evolution shows that both local and regional salinization is driven by local geology and intensive coal mining activities. The neutralization capacity of the parent geological formation buffers the acidity and lowers the overall trace element enrichment. The potential of natural weathering could be further explored as a solution to coal mining's impact on the environment.

Keywords Salt Range · Coal aquifer · Carbon mineralization · Water–rock interactions · Salinity hazard · Geological evidence

Supplementary Information The online version contains supplementary material available at https://doi.org/10.1007/s10653-023-01621-9.

N. Masood (✉) · A. Farooqi (✉)
Environmental Geochemistry Laboratory, Department of Environmental Sciences, Faculty of Biological Sciences, Quaid-I-Azam University, Islamabad 45320, Pakistan
e-mail: masood.noshin@gmail.com

A. Farooqi
e-mail: afarooqi@qau.edu.pk

K. A. Hudson-Edwards
Environment and Sustainability Institute and Camborne School of Mines, University of Exeter, Penryn TR710 9EZ, UK

T. Zafar
School of Earth and Space Sciences, Peking University, Beijing 100871, China

T. Zafar
Institute of Geochemistry, Chinese Academy of Sciences, Guiyang 550081, China

Introduction

Water is the most worrying and hostile aspect of coal mining (Ochieng et al., 2015; Wright et al., 2017). The well-known and far-reaching water footprints of coal mining are depletion of water quality, production of acid mine runoff, water–rock interaction, salinization, and the release of toxic elements. These mining impacts are roughly divided into two main mechanisms via the simultaneous incidence of acid mine drainage and subsequent water–rock interactions, which are facilitated by an acidic or alkaline pH value that promotes the release of trace elements (Mohanty et al., 2018).

Oxidation of sulfide minerals during coal mining results in acidic water and acidic mine runoff that seeps into local geology and adversely affects the hydro-geological environment in mining areas (Obiadi et al., 2016; Ross et al., 2018). This mixing and continuous influx of acid mine drainage (AMD) with groundwater and surface water changes the pH and EC and promotes the mobilization of various toxic elements. These mobile toxic metals contaminate the aquifers below as they penetrate through cracks. This flow can persist in and around more than 10 km from the source (Singh et al., 2018), which can continue to flow into neighboring aquifers and soils and affect groundwater quality. These results limit water use in household, irrigation, and industrial sectors (Jain, 2012).

In addition to these effects, another questionable aspect of the coal bed aquifer is the production of saline water, which can create a salinization risk for other groundwater (Williams et al., 2012). Salinity problems in the mining industry are due to the dissolution and mobilization of carbonates and sulfates (Nordstrom et al., 2015). The alkalinity induced by the carbonate mineralization could be an aid to mining. The coal mining impacts, i.e., natural neutralization capacity reduces toxic metal enrichment and atmospheric carbon fixation (Ross et al., 2018).

In the semi-arid to arid region of the Indus basin (Punjab), the Salt Range is one of the most important coal mining areas in Punjab. The Salt Range coal mines are extensively exposed in areas with complex geology. Some studies have shown that complex geological features, e.g., the existence of carbonaceous shale, dolomite, and other minerals have a high cation exchange capacity (Okiongbo & Akpofure, 2014). Intense mining in such geological formations can affect the natural flow, replenishment pattern, residence time, and hydraulic gradient of the water (Negrel et al., 2011; Nordstrom, 2008), resulting in negative changes in water quality, such as acidic or highly alkaline pH values as well as high TDS, trace element load and salt content in the regions. The long history of coal mining, soil degradation, and living conditions in the Salt Range area has the potential to alter the quality of aquifers. So far, only a few studies have been carried out in this area that show an acidic pH value with higher SO_4^{2-}, turbidity, TDS, salinity, Ca^{2+}, Fe, Cr, and Cu concentrations (Arshad et al., 2015; Batool et al., 2018; Jabbar Khan et al., 2020; Masood et al., 2021; Shah, 2005). The present study area is neglected, and less attention has been given to understanding the role of major ion chemistry in the formation and evaluation of salinity dynamics and the assessment of health risks. In contrast to the other environmental stressors, the origin and development drivers of salinity are extraordinarily complex and its impact on natural ecosystems was unknown. In addition, the possible potential of passive carbon mineralization could be a natural control toward carbon sequestration. Therefore, in the current complex geological framework scenario, it is hypothesized that extensive coal mining activities in this area trigger the bedrock minerals with high cation exchange capacity, which could lead to long-lasting salinization and halt the diffusion of toxic metals into the environment. Spatial distribution and health risk assessment of major anions in coal-based aquifers from the Salt Range, Punjab, has already been published (e.g., Masood et al., 2021). The present work was further devised to depict the natural neutralization capacity and its contribution to groundwater chemistry evolution. To the best of our knowledge, this study represents the first attempt to construct a conceptual model that simultaneously highlights the geochemical dynamics of salinity and the natural neutralization ability that controls the groundwater environment. This information could also provide a baseline for the formulation of future management policies as well as the carbon mineralization potential of coal mining areas with an intricate geological framework.

Geology of the study area, lithologic units, and stratigraphy

Salt Range of Pakistan, a stretch of < 180 km, lies at the foothills of the Himalayan Mountains and is bordered by the Indus (in the west) and Jhelum River in the east. The Indus River intersects the Salt Range and divides it into the main Salt Range and the Trans-Indus Salt Range (Ghazi & Mountney, 2011). Geologically, the active orogeny of the youngest Himalayas (Potwar basin) was the product of the continuous collision of Indo-Eurasian plates, which shows the sedimentary sequence of the Precambrian until the Holocene (Rehman et al., 2016). The lithology of this sedimentary sequence of the Salt Range includes sandstone, siltstones, conglomerates, clays, coals, marl, gypsum, shale, rock salt, dolomite, and chalcopyrite, (Malkani & Mahmood, 2017). Where coal, marl, gypsum, rock salt, and dolomites are the soluble minerals that can alter the hydrochemistry of the area (Shah et al., 1993). It is sparsely populated with main settlements that were around the mining sites. Where the livelihood is coal, limestone mining, limestone quarries, and limited agriculture. The inhabitants of these areas are dependent on groundwater for domestic, industrial, and irrigation purposes.

The Paleocene stratigraphy and lithofacies include Hangu, Patala Formation, and Lockhart Limestone (supplementary data Figure S1). During the late Paleocene, the development of a lacustrine environment in the Eastern and Central parts of the Salt Range produced a workable coal seam of the Patala Formation. The 18–20 m thick Patala coal seams of the main Salt Range are embedded laterally and vertically with hydrocarbons as a single discontinuous bed. Coals of the Patala formation lie near the surface and are sandwiched between an upper limestone unit and a lower shale unit. Mining activities in the Salt Range are limited to the eastern (ESR), and central (CSR) parts (Fig. 1a). The ESR extends from Ara to Nilawahan, but the notable coalfields are only confined to Ara (Basharat) and Dandot areas (Rehman et al., 2016). Therefore, coal mining areas in and around Ara Basharat and Dandot are considered for the present study. CSR's selected coal mines are Padhrar (PC), Katta Karli (KR), Arrara (AC), and Munarah (MC). Another workable coal bed in the Trans-Indus Salt Range (TSR) is documented in the Hangu Formation. Coal deposits of the Hangu Formation spread over the laterite layer and underlying shale and siltstone. The main coal seam is 0.5–3.5 m long. About 20 m above the main seam, another coal seam of 1.5 m with a lateral extension of 300–400 m is found in this region. This coal seam is further embedded with shale and sandstone. Coal-mining activities in TSR's Hangu formation are limited to Makarwal (MK) and its surrounding area, mined from the western edge of the Makarwal anticline (Fig. 1b). These coals are related to oxysols and coastal sediments and are of better quality than the Patala coals, which are related to marine sediments that contain clayey mineralogy such as kaolinite and illite (Warwick & Wardlaw, 2007).

Regional hydrology

The Paleocene coal-bearing units consist of sandstone, shale, coal, and carbonaceous shale and are laterite and bauxite of the Indus Formation. This formation has permeable sandstone, which may be aquiferous; hence, the adjacent coal seams may have water as well. However, the clays/shale beds are not permeable and therefore, cannot store water, which makes the seepage of rainwater the primary pathway for groundwater recharge. Evapotranspiration and exploitation through water wells for local and industrial consumption are the main discharging mechanisms. The hydrology of the TSR is mainly controlled by the Indus River as it lies at a higher elevation and its coarse-grained sediment deposits re-enrich the groundwater in this area (Hussain et al., 2017). The local geological formations of the Salt Range favor the hydrological gradient for recharge and discharge patterns. The climatic conditions are dry to semi-arid with an average annual rainfall of 300–800 mm (Hussain et al., 2019; Jabbar Khan et al., 2020). The average annual evapotranspiration (ET), estimated by the horticultural station in Soan–Sakesar Valley (CSR), is 2.6 mm/day (with a range of 1.5–6.4 mm/day) (Hussain et al., 2019). The main drainage zones in the study area are the floodplains of the Indus and Jhelum Rivers, where parallel drainage patterns have been observed. The water table in the Salt Range is generally shallow, with a depth of 4 and 7 m below the surface, but in recent years excessive extraction of groundwater has deepened the water table to below 10 m (Hussain et al., 2019). The alluvium of the Salt Range consists of a mixture of sand and clay with a

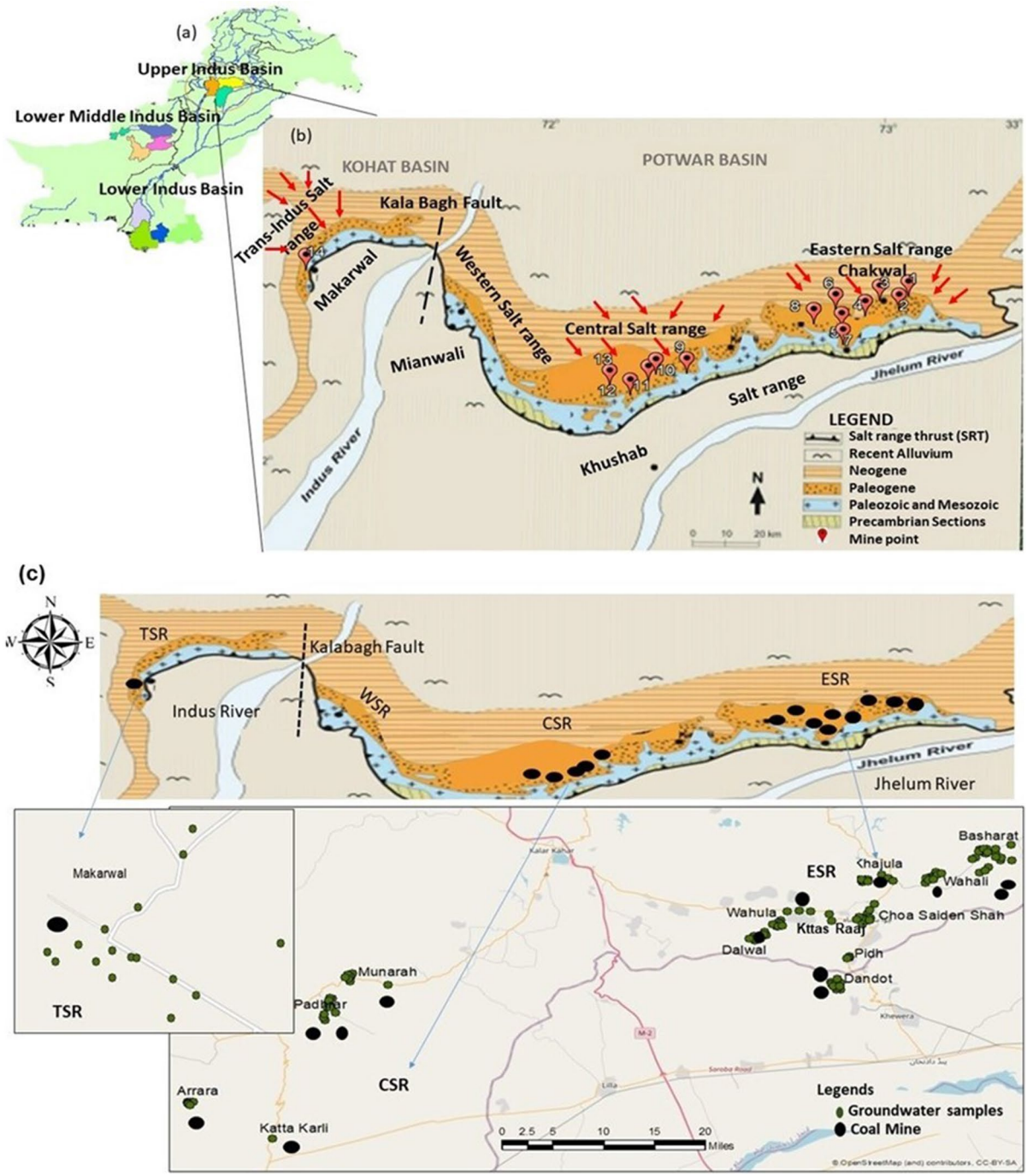

Fig. 1 **a** Map of Pakistan presenting three main coal-producing areas. **b** Geological map with sampling sites of coal mining areas of the Salt Range, Punjab (modified after). *Red arrowhead shows the drainage pattern in the area. **c** Groundwater sampling locations and sampling points in the study area. *ESR = eastern Salt Range, CSR = central Salt Range, WSR = western Salt Range, TSR = Trans-Indus Salt Range

discontinuous proportion of 25–35% of clay layers and 65–75% fine to coarse-grained sand. The spatially continuous sand layer mainly comprises quartz minerals with good porosity and permeability values, which generally influence the hydrochemistry in the area (Hussain et al., 2017).

Materials and methods

Collection and analysis of groundwater samples

To determine the water quality of coal mining areas, 131 groundwater samples were collected from existing wells/boreholes in the entire Salt Range, i.e., the eastern Salt Range (ESR) (Chakwal), the central Salt Range (CSR) (Khushab), and Trans-Indus Salt Range (TSR) (Makarwal) (Fig. 1c). The water sampling was based on the population density in these mining areas. From the ESR area, 97 groundwater samples from 9 densely populated villages Dalwal (DLC), Basharat (BT), Khajula (KHC), Wahali (WIC), Wahula (WAC), Pidh (PIC), Dandot (DTC) Kattas Raaj (KR), and Choa Sayidan Shah (CS) were collected. However, 23 samples were collected from four locations including CSR (Munarah (MC), Arrara (AC), Padhrar (PC), and Katta Karli (KC); and 11 samples from the TSR location Makarwal (Mk) (Fig. 1c). The coordinates of mines and groundwater samples are provided in the supplementary data (Table S1). Flushing was conducted until pH and EC were constant before the samples were taken, which were then filtered with 0.45 µm membrane filters. The pH, EC, and TDS were measured in situ with a portable multi-element meter (HANNA). Water samples were then divided into two sets, one set was acidified with concentrated HNO_3 for trace elements and cations, and another was left non-acidified for anion analysis. The samples were then shifted to the Environmental Hydro-Geochemistry laboratory at Quaid-i-Azam University Islamabad for further analysis. The major cations analysis was performed by atomic absorption spectroscopy (Agilent 55AA) following the methods of the American Public Health Association (APHA)(Federation, 2005). Bicarbonates were analyzed using acid–base titration using 0.1N HCl. SO_4^{2-}, NO_3^-, PO_4^{3-}, F^-, Cl^-, and Br^- ions were measured by ion chromatography (thermo dual channel ICS-5000 + Ion chromatography system) at the University of Leeds, UK. However, trace metals were analyzed using inductively coupled mass spectrometry (ICP-MS) at the Camborne School of Mines, Environmental Sustainability Institute, University of Exeter, Penryn Campus, Exeter, UK. To verify the electro-neutrality, the ion balance (IB) was calculated, and all samples had an IB value of ±5% (supplementary data, Table S2). The total hardness of $CaCO_3$ was calculated using the equation (Federation, 2005) (Eq. 1).

$$\text{Totalhardness}(CaCO_3\text{ppm}) = (Ca * 2.50) + (Mg * 4.12) \quad (1)$$

The salt hazard of irrigation water in terms of sodium adsorption ratio (SAR), soluble sodium percentage (Na^+%) (SSP), magnesium adsorption ratio (MAR), Kelly ratio (KR), and potential salinity (PS) was determined using the following equations (Doneen, 1964; Richards, 1954; Wilcox, 1955) (Eqs. 2–6).

$$\text{SAR} = \frac{Na^+}{\sqrt{\frac{1}{2}\left(Ca^{2+} + Mg^{2+}\right)}} \quad (2)$$

$$\text{SSP} = \frac{\left(Na^+ + K^+\right) * 100}{\left(Ca^{2+} + Mg^{2+} + Na^+ + K^+\right)} \quad (3)$$

$$\text{MAR} = \frac{Mg^{2+} * 100}{Mg^{2+} + Ca^{2+}} \quad (4)$$

$$\text{KR} = \frac{Na^+}{Ca^{2+} + Mg^{2+}} \quad (5)$$

$$\text{PS} = Cl^- + {}^1/_2 SO_4^{2-} \quad (6)$$

where KR > 1 means an excess of Na ions in water. KR < 1 indicates the suitability of water for irrigation purposes and KR > 3 shows that the water is not suitable for crop irrigation.

To understand the natural buffering against acidification induced by coal mining, the acid neutralization capacity (ANC) of the coal bed aquifers was calculated using the equation (Eq. 7).

$$\text{ANC} = \left(Ca^{2+} + Mg^{2+} + K^+ + Na^+\right) - \left(SO_4^{2-} + Cl^- + NO_3^-\right) \quad (7)$$

The ionic concentrations were taken in milliequivalents.

Table 1 Statistical summary of groundwater parameters with the minimum (min), maximum (max), mean, and standard deviation (SD) in coal-based aquifers of Salt Range, Punjab

Parameters	Units	WHO limit	Eastern Salt Range ($N^a=9$) ($n^b=97$)				Central Salt Range ($N=4$) ($n=23$)				Trans-Indus range ($N=1$) ($n=11$)			
			Min	Max	Mean	SD	Min	Max	Mean	SD	Min	Max	Mean	SD
Depth	Meter	–	6	122	56.3	25.9	21	137	70.7	43	131	142	137	33
pH	–	6.5–8.5	7.0	8.6	7.7	0.26	5.7	7.6	6.6	0.6	8.0	8.8	8.3	0.7
EC[c]	µS/cm	1500	430	2910	1190	447	330	1290	566	260	1270	1740	1566	343
TDS[d]	mg/L	1000	312	2050	839	308	234	920	404	183	894	1290	1153	261
TH[e]	mg/L	< 120	322	733	498	87.5	147	703	395	118	408	738	512	101
Na^+	mg/L	200	2.7	84.8	25.1	17.8	16.6	389	92.7	107	134	210	166	25
K^+	mg/L	12	0.3	54.5	8.1	11.3	2	41.6	7.2	11.3	1.3	12	5.2	2.7
Ca^{2+}	mg/L	75	17.5	158	117	30	31	183	98.8	33.9	46	70.8	58.2	7.5
Mg^{2+}	mg/L	50	8	98.6	49.3	20.3	16.8	59.3	35.1	12.5	56	148	89	24.6
Cl^-	mg/L	250	0	424	110	97.3	6.2	423	77.2	108	38	230	102	59.7
HCO_3^{-f}	mg/L	–	100	500	300	89.3	100	400	319	50.5	200	450	368	68
SO_4^{2-}	mg/L	250	14	190	90	45	30	580	144	148	160	618	314	137
NO_3^-	mg/L	50	0.2	308	58.5	57.7	2.7	203	73.4	67.5	1.1	259	64.8	82.7
PO_4^{3-}	mg/l	0.1	–	–	–	–	–	0.2	0.0	0.1	–	–	–	–
Fe	mg/L	0.3	0.6	9.2	3.5	0.3	0.5	1.3	1.0	0.3	2.5	3.3	1.8	–
As	µg/L	10	–	0.7	0.7	–	0.0	1.8	0.1	0.4	1.3	3.6	2.4	1.6
Br^-	mg/L	–	–	14	2.1	3.5	–	0.5	0.1	0.1	–	–	–	–
F^-	mg/L	1.5	0.1	1.8	0.6	0.5	0.1	2.7	0.9	1	0.3	2.5	1.6	1.0
Mn	mg/L	0.5	–	1.2	1.2	0.1	–	0.0	0.0	0.0	–	–	–	–
Cu	mg/L	2	–	0.9	0.7	0	–	–	1.5	0.3	–	0.0	0.0	0
Zn	mg/L	5	–	4	3.2	0.7	0.1	6.6	4.2	0.2	0.1	7.5	3.7	–
Pb	mg/L	0.01	–	–	–	–	–	–	–	–	–	–	–	–

*[a]N = sampling sites, [b]n = sample number, [c]EC = electrical conductivity, [d]TDS = total dissolved solids, [e]TH = total hardness as $CaCO_3$, [F]HCO_3^- = alkalinity as $CaCO_3$

"–" below detection limit, i.e., Mn = 0.001, Fe = 0.05, Cu = 0.002, Zn = 0.001, Pb = 0.01 mg/L As = 0.04 µg/L

Results and discussion

Geochemistry and quality evaluation of groundwater for drinking purposes

Groundwater chemistry and spatial distribution of physico-chemical parameters in the coal-based aquifers from Salt Range, Punjab, are given in Table 1. The pH of the ESR and TSR water samples ranged from 7.0 to 8.8 with an average value of 7.7, while the pH of CSR ranged from 5.7 to 7.6 with an average value of 6. The EC values of all sites were within acceptable limits of 1500 µS/cm (Reddy et al., 2014; Zhang & Qin, 2018) except for Dalwal (ECR site) with EC value of 2910 µS/cm. The total dissolved solids contents (TDS) of the ESR ranged between 312 and 2050 mg/L with an average value of 839 mg/L (Table 1). TDS concentrations for CSR water samples varied from 234 to 920 mg/L with an average value of 404, and in the case of the TSR site, the TDS values ranged from 894 to 1290 mg/L (average value of 1153 mg/L). Freeze and Cherry (1979) classify water into four categories, water with TDS < 1000 mg/L as freshwater, > 1000 mg/L as brackish water), > 10,000 mg/L as saline water, and 100,000 mg/L as brine. Following this classification, 76% of the water in ESR is fresh and safe to drink while 24% of the samples are brackish. While at TSR about 90% of these water samples are brackish and unsuitable for drinking purposes (Table 1). In the case of CSR, however, the TDS value was < 1000 mg/L referred to as freshwater's had relatively low TDS (Table 1). The

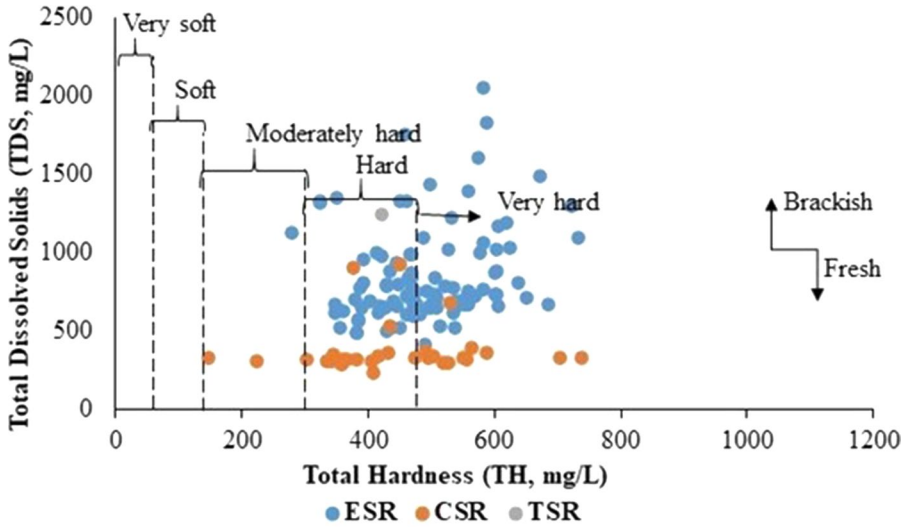

Fig. 2 The status of groundwater hardness in coal mining areas of Salt Range, Punjab

spatial differences between the TDS values could be attributed to the variation in geochemical processes and anthropogenic activities at three different locations in the region (Table 1). The calculation of the total hardness (Fig. 2) shows that water samples are ridiculously hard at all locations except at one site (Arrara of CSR) which has moderately hard water.

The main cations in CSR and TSR were $Na^+ > Ca^{2+} > Mg^{2+} > K^+$ and $Na^+ > Mg^{2+} > Ca^{2+} > K^+$, respectively, while the order for ESR followed the sequence $Ca^{2+} > Mg^{2+} > Na^+ > K^+$ (Table 1). The average total cation strength (TZ+) showed that the proportion of sodium percentage (Na^+%) (12% of ESR, 33% of CSR) is relatively lower than calcium (Ca^{2+} %) (i.e., 59%, 48% for ESR, and CSR, respectively). However, the TSR site shows the opposite behavior with 52% Na% and 19% Ca^{2+}% distribution. For CSR and TSR, Na^+ is the most dominant cation with 16.6–389 mg/L (average 92.7 mg/L) and 134–209 mg/L with an average value of 165.8 mg/L. About 90% of ESR samples and 78% of the CSR samples exceeded the WHO recommended values of 75 mg/L for Ca^{2+}. Similarly, 45% of the ESR and 17% of the CSR wells exceeded Mg^{2+} concentrations of more than 50 mg/L (WHO, 2011). In the case of TSR all wells (with a range of 56–148 mg/L the Mg^{2+} ion concentrations exceeded the WHO limit of 50 mg/L (Table 1), the Ca^{2+} concentrations for the TSR site were, however, within the permissible limit of 75 mg/L. The increased concentrations of Ca^{2+} and Mg^{2+} in the study areas are likely derived from dolomite, gypsum, limestone, sandstone, and conglomerate, i.e., the geological formations of the Miocene and Paleocene (supplementary data Figure S1) (Bouteraa et al., 2019; Masood et al., 2022). While the dissolution of sodium-bearing minerals (such as halite) results in higher sodium levels in the aquifers of CSR and TSR. Low sodium content in calcite-rich aquifers of ESR could be due to the replacement of Na^+ by cation exchange. However, dissolving limestone could intensify this process (supplementary data Table S3).

The potassium concentrations were in a range of 0.3–54.5 (average 8.1 mg/L) and 2.0–41.6 mg/L (average 7.2 mg/L) in ESR and CSR sites, which were above the WHO limit, i.e., 12 mg/L on the other hand, TSR values for K were within the permissible limits of 12 mg/L (Table 1). The cause of these K^+ concentrations can be attributed to the occurrence of silicate minerals such as feldspar and jarosite in the study area (Ghazi & Mountney, 2011).

The main anionic configuration showed the sequence of $HCO_3^- > Cl^- > NO_3^- > SO_4^-$ in the ESR. In contrast, the CSR and TSR followed the enrichment pattern of $SO_4^{2-} > HCO_3^- > NO_3^- > Cl^-$ and $SO_4^{2-} > HCO_3^- > Cl^- > NO_3^-$ (Table 1). HCO_3^- concentrations at ESR, CSR, and TSR locations were 100–500, 100–400, and 200–450 mg/L, respectively. Groundwater SO_4^{2-} of ESR was within the WHO limit of 250 mg/L. However, the SO_4^{2-} concentrations in CSR (30–580 mg/L) with an average value of 144 mg/L and TSR (160–618 mg/L) with an average value of 314 mg/L wells were higher (Table 1). These elevated levels of SO_4^{2-} values are globally

recognized as indicators of coal mining activities (Bosman, 2009). In the case of the present study area, gypsum, the primary source of SO_4^{2-} is most likely related to the lithology of the area (Hussain et al., 2015); Higher SO_4^{2-} concentrations resulted from re-enrichment of precipitation, where groundwater flows through the thick limestone, gypsum-bearing minerals, and sulfurous coals of the Salt Range (Long & Luo, 2020; Masood et al., 2022).

Around 11% of the ESR and 9% of the CSR groundwater samples exceeded the WHO limits of 250 mg/L for Cl^- (Table 1). Elevated Cl^- values were sourced either from rock salt or coals (Batool et al., 2018; Finkelman et al., 2019). Under the alkaline water, the huge rock salt deposits in the Salt Range mainly add higher Na^+ and Cl^- to the groundwater. Similarly, chlorine-enriched halides (such as halite and sylvite) and organic matter have also been observed in coals too (Finkelman et al., 2019; Mazurek et al., 2020).

The NO_3^- contamination of the groundwater is one of the most important drinking water problems in the study area. NO_3^- concentrations vary between 0.2–308 (average value of 59 mg/L), 2.7–203 (average value of 73 mg/L), and 1.1–259 mg/L (average value 65 mg/L) for the CSR, ESR, and TSR wells, respectively (Table 1). About 42% of the ESR, 52% of the CSR, and 36% of the water samples from TSR sites exceeded the WHO limit value of 50 mg/L for NO_3^- (WHO, 2011). Typically, groundwater NO_3^- contamination is mainly sourced from agricultural and sewage sources and retained in shallow water (Qurat-ul-Ain et al., 2017). In addition, biological nitrogen fixation and the use of explosives in mining areas are possible sources of nitrate (Bosman, 2009; Li et al., 2018; Mahmood et al., 2017).

Fluoride is another important pollutant in the study area. The detected F^- concentrations in the Salt Range. Fluoride concentrations in the groundwater of ESR samples were in the range of 0.1–1.8 mg/L with only 3% of the samples exceeding the permissible limit of 1.5 mg/L (WHO, 2011). However, 17% of the samples at CSR and 27% of the TSR groundwater samples were above the F^- values of the WHO limit value of 1.5 mg/L (Table 1). The accumulation of F^--containing minerals such as apatite, fluorite, biotite, and mica has been found within the mineralogy of the Salt Range area (Masood et al., 2020, 2021). Since the geology of the Salt Range is rich in limestone, the alkaline pH favors the dissolution of these carbonates, which can improve F^- mobility. The salinization/salt effect could also favor F^- contamination. The dissolution of halite, gypsum, or salt-water presence in the Salt Range area can increase ion concentration and form F^- complexes with Mg^{2+}, Ca^{2+}, and Na^+ ions, which reduce the activity of the groundwater F^- and activate the dissolution of F^--containing minerals (supplementary data, Table S3). The negative correlation of F^- and Ca^{2+} and positive correlation with Na^+ also showed that the dissolution of fluoride-containing minerals and the subsequent cation exchange of Na^+ and Ca^{2+} ions mobilize the F^- content in the groundwater (supplementary data, Table S4a, b & c). Elevated levels of major cations and anions and their geochemical profiles were also well established (Masood et al., 2021). The present study was further built up on the same dataset of (Masood et al., 2021) to explore hydrochemical classification, natural mineralization, and its potential impact on crop production as well as its potential for carbon sequestration.

Hydrogeochemical classification and origin of solutes

The Piper trilinear diagram, based on the relative concentrations of major cations and anions, classifies the water types as Ca–Mg–Cl, Ca-HCO_3, and Ca-Cl_2 in the ESR with 72% of the samples as the Ca-HCO_3 type. In CSR, Ca-HCO_3 (69%) is the dominant water while 17% falls in Na-Cl and 14% is Ca-Cl_2 and Ca-Mg-Cl_2 (Fig. 3a). In the case of TSR, 73% of the samples are Ca-Mg-Cl_2 and 23% are of the mixed type of Ca-Mg-SO_4 and Ca-Cl_2 (Fig. 3a). In all groundwater samples, the alkaline earth metals (Ca^{2+} + Mg^{2+}) exceeded the alkali metal cations (Na^+ + K^+) (Table 1). The plotted points of the ESR and TSR groundwater samples that fall in field 2 indicate carbonate hardness. Certain factors determine the chemical quality of the groundwater such as the geological structure and mineralogical composition of the aquifer, rainwater, duration of the water–rock interaction, dissolution and precipitation of mineral species, and anthropogenic influences (Singh et al., 2008). Gibbs' diagram showing the ratio of $Na^+ + K^+/(Na^+ + K^+ + Ca^{2+})$ and $Cl^- + NO_3^-/(Cl^- + NO_3^- + HCO_3^-)$ as a function of TDS is used to determine the functional sources of dissolved chemical constituents, such as precipitation,

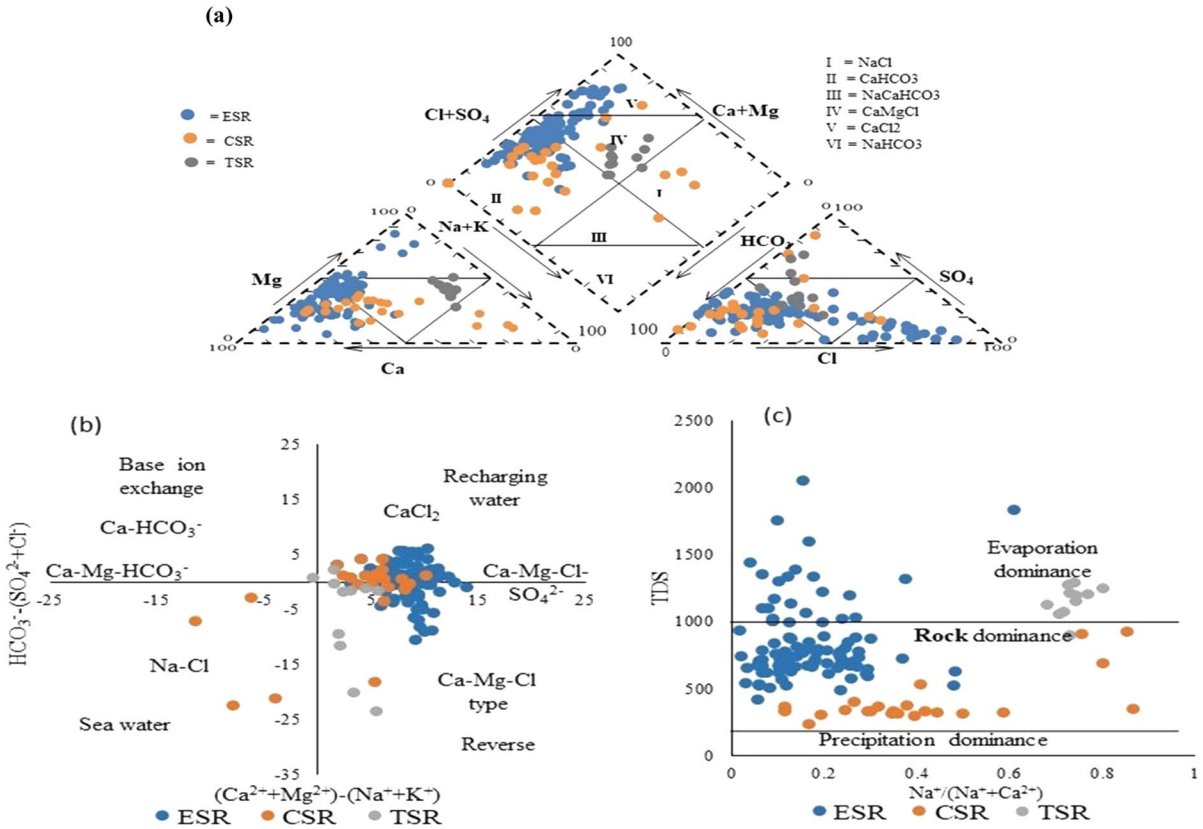

Fig. 3 **a** The Piper plot, **b** Chadha diagram (modified piper plot) and **c** Gibbs plotting of groundwater around coal mining areas of Salt Range

rock, or evaporation dominance (Gibbs, 1970). The graphic representation of Gibb's diagram indicates that rock weathering is the dominant controlling factor in groundwater development (Fig. 3c) which is in agreement with the other studies (e.g., Okiongbo & Akpofure, 2014). Whereas some samples are in the evaporation area, pointing out that the hot and semi-arid climate of the study area favors the evaporation process, which could also affect the groundwater chemistry (Fig. 3c).

The Chadha diagram (Fig. 3b) was used to evaluate water types of ESR, CSR, and TSR to determine the major mechanisms that control water chemistry (Bouteraa et al., 2019). Most of the samples plotted against $HCO_3^- - (SO_4^{2-} + Cl^-)$ versus $(Ca^{2+} + Mg^{2+}) - (Na^+ + K^+)$ grouped around field 1 showed that the dissolution of minerals and reverse ion exchange as a major hydro-geochemical control of groundwater chemistry. However, fewer samples from CSR sites showed evaporation-dominating processes (Fig. 3b). Under favorable conditions, the dominant cations go through the exchange mechanisms. Reverse cation exchange is a process in which Na^+ ions in the aqueous solution are replaced by Ca^{2+} and Mg^{2+} ions (Bouteraa et al., 2019). We propose that the overall lower percentage contribution of the Na^+ ion to the cationic strength (i.e., 12% for ESR and 33% for ESR) compared to Ca^{2+} (52% and 48% for ESR and CSR, respectively) demonstrates the replacement of Na^+ ions and represent reverse cation exchange mechanism. In the case of the TSR site, however, a higher Na^+ (52%) and a low Ca^{2+} (19%) content show the exchange of aqueous Ca^{2+} ions in the groundwater and demonstrate the cation exchange. This pattern is further complemented by the dominance of Ca–Mg–Cl, Ca–Cl_2, and Ca–Mg–HCO_3 water in the present study area illustrating reverse cation exchange processes (Fig. 3b). Alkaline earth metals (Ca^{2+} and Mg^{2+}) outperform the alkali metals (Na^+ and K^+) indicated that strongly

acidic anions dominate over weakly acidic anions and are characterized by the weathering and dissolution of rocks (Fig. 3c) (Singh et al., 2019). Mixing of freshwater with mine water could produce Ca–Cl_2-type water (Singh et al., 2019; Yadav et al., 2020). The bedrock deposits of limestone and dolomite via reverse ion-exchange mechanism and the oxidation of gypsum and pyrite due to accelerated coal mining in the ESR and CSR sites, recharge the area with water of Ca–HCO_3 type (Dlamini & Demlie, 2020). A few CSR wells with Na-Cl-type water with higher alkalis support the evaporation mechanism (Saou et al., 2012).

In addition, ion chemistry has been widely used to infer the main hydrogeochemical processes that take place in the aquifer. The relationship between Na^+ and Cl^-has often been used to identify the mechanism for salinity in semi-arid to arid regions. When the molar ratios in the groundwater are close to 1.0, it suggests that the dissolution of halite is the main source of Na^+ and Cl^-. The higher Na^+/Cl^- ratio (> 1.0) indicates a non-halogenated source and suggests silicate weathering as a source of Na^+. In the case of TSR, water samples have molar ratios > 1 (Fig. 4a) suggesting that Na^+ has other major sources, such as the cation exchange (Na^+ to Ca^{2+} exchange) and silicate weathering reactions (Guo et al., 2007). However, a poor correlation between Na^+ and HCO_3^- ($r = 0.3$) (supplementary data Table S4a, b, c), indicates that Na^+ concentrations were probably weakly influenced by silicate weathering (Cheung et al., 2010). Few samples of ESR and CSR (17%) are on the 1:1 line indicating halite dissolution as the main source. However, the majority of ESR groundwater samples have a Na^+/Cl^- ratio < 1 implying that the dissolution of other chlorite salts is the main reason for the increased Na^+ and Cl^- concentrations (Fig. 4a). The ratio of Cl^-/Br^- (ranged 0.29–4550) also reinforced that evapotranspiration-assisted halite dissolution and increased Na^+ and Cl^- concentrations (Table 1).

The ratio of (Na^+–Cl^-) versus ($Ca^{2+} + Mg^{2+}$)–($HCO_3^- + SO_4^{2-}$) is generally used to determine the ion exchange process (Chen et al., 2020). If cation exchange is an important control process for groundwater, the relationship between (Na^+–Cl^-, meq/L) and ($Ca^{2+} + Mg^{2+}$)–($HCO_3^- + SO_4^{2-}$meq/L) should be linear with a slope of −1.0. Figure 4b shows that all water samples were distributed around the line, which is more pronounced for ESR ($r^2 = 0.8$)

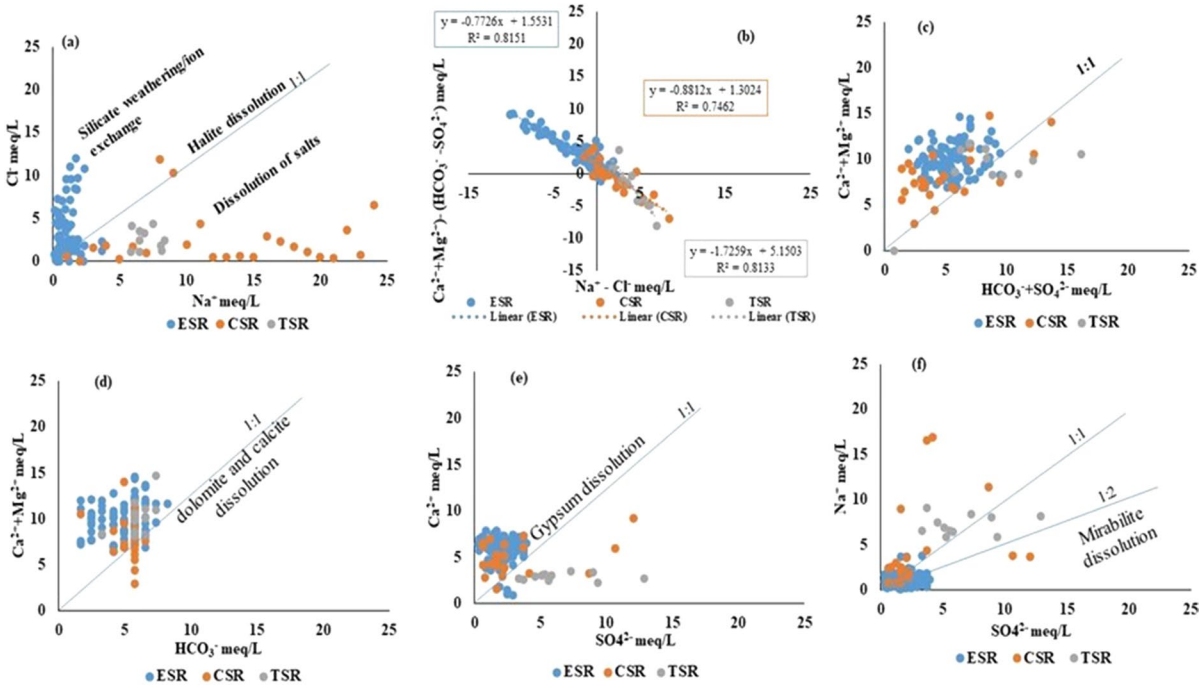

Fig. 4 Bivariate plots of different ionic concentrations in groundwaters of Salt Range aquifers

and TSR ($r^2 = 0.8$) compared to CSR ($r^2 = 0.7$) revealing the participation of Ca^{2+}, Mg^{2+}, and Na^+ ions in exchange reaction. Whereby TSR with high concentrations of Na^+ ion and lower values of Ca^{2+} and Mg^{2+} suggested a cation exchange process (as described above). In comparison, increased Ca^{2+} and Mg^{2+} ions in the ESR and CSR sites indicated depletion of Na^+ concentrations via a reverse ion exchange mechanism (Fig. 4b and Table 1).

If Ca^{2+}, Mg^{2+}, SO_4^{2-} and HCO_3^- in groundwater are derived from a simple mixture of the dissolution of dolomite, gypsum, and calcite, the plot of ($Ca^{2+} + Mg^{2+}$) versus ($HCO_3^- + SO_4^{2-}$) is close to 1:1 line. In this study, few samples of CSR (20%) and ESR (15%) fall below the 1:1 line while most of the samples are above the 1:1 line (Fig. 4c) indicating that Ca^{2+}, Mg^{2+}, SO_4^{2-} and HCO_3^- of the groundwater are partially obtained from the dissolving dolomite, gypsum, and calcite, and the excess negative charge of HCO_3^- and SO_4^{2-}must be balanced by Na^+. Since the described reverse cation exchange prevailed against higher concentrations of $Ca^{2+}$and Mg^{2+} ions, this can also make the data points move away from the 1:1 line of ($SO_4^{2-} + HCO_3^-$, meq/L) versus ($Ca^{2+} + Mg^{2+}$, meq/L).

Figure 4d shows that about 15% of the groundwater samples fall on or near the 1:1 line of HCO_3^- (meq/L) versus ($Ca^{2+} + Mg^{2+}$, meq/L), and the line represents the dissolution of dolomite and calcite (carbonate minerals) by H_2CO_3. However, a large part of the samples are above and to the left of the line, indicating excess Ca^{2+} and Mg^{2+} due to the dissolution of sulfate or reverse cation exchange of Na^+-Ca^{2+}; some samples below and to the right of the line, indicating excess HCO_3^- likely sourced from other processes such as silicate weathering (e.g., plagioclase), and methyl-fermentation process in the coal seam (Whiticar, 1999), that can generate CO_2 and then form HCO_3^-. To see the influence of the gypsum dissolution on the composition of the groundwater, SO_4^{2-} was plotted against Ca^{2+} in (Fig. 4e), showing that only about 10% of the samples from ESR and CSR fall on the 1:1- line, and reflects the dissolution of gypsum. All samples of TSR are below and to the right of the line, that is typically interpreted as an excess of SO_4^{2-}originating from other processes such as pyrite oxidation (Tarki et al., 2011). Coal mining activities create an oxidizing environment, that leads to the oxidation of pyrite in the coal seam and the formation of SO_4^{2-}, and the reaction is as the following equation (Eq. 8) (Masood et al., 2022).

$$4FeS_2 + 15O_2 + 14H_2O = 14Fe(OH)_3 + 8SO_4^{2-} + 16H^+ \quad (8)$$

In addition, supplementary data Table S4b and Fig. 4f show that SO_4^{2-} has a good positive correlation ($r = 0.6$) with Na^+ in TSR, and some groundwaters (approx. 22%) from ESR and CSR on the 1:1 line stands for mirabilite dissolution, suggesting that the mirabilite dissolution can also be one of the sources for SO_4^{2-}.

Metal concentrations and a driver behind elevated concentrations

Among the major and trace metals, Fe, As, Cu, Mn, Pb, and Zn in the groundwater of the study area were analyzed (Table 1). Overall, the Fe concentrations of 68% of the ESR, 87% of the CSR, and 36% of the TSR samples were above the WHO limit value of 0.3 mg/L. Mn with 2% samples having a concentration above the WHO limit of 0.5 mg/L was only detected in the ESR site. Similarly, higher Zinc values were reported in 9% of the CSR and TSR wells which is above the WHO limit of 5 mg/L (Table 1). As and Cu were within the permissible limits of 0.01 mg/L and 2 mg/L at the ESR, CSR, and TSR sites, while the Pb concentrations at all sites of ESR, CSR, and TSR were below the respective detection limit of 0.1 mg/L (Table 1). We propose that the oxidation of pyrite could be the source of these elements (Arshad et al., 2015; Li et al., 2014; Masood et al., 2022; Sahoo & Khaoash, 2020).

The control agents behind the lower or below the detection limit (bdl) of these trace elements such as As, Cu, Mn, and Pb is the saturation of alkaline minerals (dolomite, gypsum, and carbonaceous minerals) (supplementary data Table S3) and alkaline pH (Wu et al., 2020). The lack of Mn concentration in TSR is related to the alkaline pH of the water at which Mn normally precipitates as oxyhydroxides. SI values indicate that carbonates are below saturation, which promotes the formation of complex agents of quartz containing Fe and Mn (Li et al., 2014). Oxidation of sulfides (pyrite) along with weathering of anhydrite, dolomite, and gypsum minerals could be a possible source of these potential water system pollutants

(Sahoo & Khaoash, 2020). In the present study area, the positive correlation of SO_4^{2-} with Ca^{2+}, Mg^{2+}, F^-, and Na^+ validates these suggestions (supplementary data, Table S4). Acidification through the oxidation of pyrite minerals releases various trace elements (e.g., As) into the surrounding environment (Masood et al., 2022; Ross et al., 2018).

Increased values of Ca^{2+} and Mg^{2+} in contrast to bicarbonate ions, which are balanced by sulfate charge, show the natural acidification status using the $Ca^{2+}+Mg^{2+}$ versus HCO_3^-diagram (Fig. 4d). Much of the samples that tend toward the 2:1 line reflect the importance of strong acids; this is likely due to rock weathering that causes dissolution and oxidation of sulfide-bearing minerals accelerated by the pronounced coal mining activities in the region (i.e., the pyritic acid) (Obiadi et al., 2016). Some samples falling around the 1:1 slope suggest that the release of weak acids due to naturally occurring biogeochemical processes also triggers the natural acidification mechanism (i.e., the production of CO_2 and carbonic acid) (Ross et al., 2018).

The sandwich nature of the present studied coals with limestone beds also causes the deliberate mixing of pyritic acid with acid-neutralizing carbonates such as calcites and silicate minerals, which prevents acid mine drainage (Tay et al., 2014). The naturally occurring acid neutralization capacity (ANC) of the groundwater (Eq. 7) at TSR (with a range of 3.6–9.6 and a mean value of 5.3) and ESR (0.1–9.3 and mean value of 5.3) were much more pronounced when compared to CSR (0.5–8.5 with a mean of 5.9).

Therefore, the highly mineralized water of ESR and TSR suppresses the temporarily occurring acidification. The neutralization capacity of the CSR site with the lowest value of (0.5–8.5) in this area had shown acidity to be the more pronounced phenomenon (Fig. 5). Overall, relatively higher concentrations of SO_4^{2-}, Ca^{2+}, and Mg^{2+} ions indicate that although acid mine water is produced in the aquifers of coal mines, the neutralization capacity of Ca^{2+} and Mg^{2+} bearing dolomite, silicate, and carbonate minerals is much more enhanced and perhaps controls the overall release of toxic elements (such as Cu, Pb, and Mn) (Table 1).

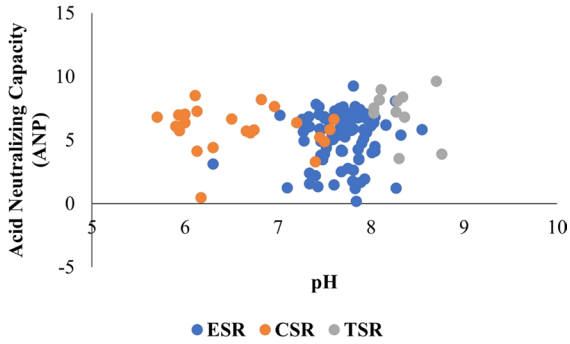

Fig. 5 Acid neutralization capacity of major groundwater ions (elemental values were taken in milliequivalents)

Groundwater quality evaluation for agriculture purposes

Being an agricultural region, the Salt Range is susceptible to constraints that may risk salinity and result in low or limited crop output. As a disruptive element and a measure of salt, Na ions can change the physical characteristics of soils and render them impermeable (Obiadi et al., 2016). In addition, the high electrical conductivity, and the level of total dissolved salts

Table 2 Summary of irrigation water parameters and their comparison with standards

Statistics	ESR			CSR			TSR			*Irrigation water guideline	
	Min	Max	Mean	Min	Max	Mean	Min	Max	Mean	suitable	Unsuitable
EC µS/cm	430	2910	1189.7	330	1290	565.7	1270	1740	1566	< 3000	> 3000
Ca^{2+}/Mg^{2+}	0.2	16	3	1	6	3	0.3	1.3	0.7	–	–
SAR	0.1	2.0	0.5	0.3	9.2	2.2	2.4	4.2	3.2	10–18	> 26
MAR	9	90	40	22	57	38	57	83	71	< 50	> 50
SSP	0.2	36	9	8	76	28	37	49	42	40–60	> 80
KR	0	0.5	0.5	0.1	3	0.6	0.5	1	0.7	≤ 1	≥ 1
PS	1	12	4	0.3	14	4	2	8	5.6	< 3	> 3

*Referenced by Wilcox (1955) and Richards (1954)

indicated salinity hazard and toxicity. The suitability of irrigated water with increased EC was measured using the sodium and magnesium adsorption ratio (SAR, MAR), sodium percentage (Na%), Kelley's ratio (KR), and potential salinity (PS) (Table 2).

The calculated SAR values were between 0.1–2 (mean value 0.5) for ESR, 1.2–2.6 with a mean value of 2.0 for CSR, and 2.4–4.2 with a mean value of 3.2 for the TSR site. Richard's plot of SAR vs EC showed that except for the fewer sample of ESR of the C4-S1 class, both ESR and TSR wells fall under the C3-S1 category (Raju et al., 2011; Richards, 1954) (Fig. 6b). In the case of CSR wells, most of the samples fall under the C2-S1 class, with less than one of the C3-S1 and only one sample of the C3-S2 class. Classes C2-S1 and C3-S1 showed that these wells had a minimal risk of SAR with a medium to substantial risk of EC. However, class C4-SI showed an extremely substantial risk of increased EC, and samples with the C3-S2 category had high Na^+ ions, which can cause prolonged salinity. On the other hand, comparatively increased magnesium concentrations as a substitute for Na^+ could become more dangerous than sodium-based salinity via the reverse ion exchange process. To counter this magnitude of the magnesium hazard, the calculated MAR of water wells showed that 27% of the ESR, 22% of the CSR, and 100% of the TSR wells were unsuitable for irrigation practices (Table 2). These observed MAR values were due to the dissolution of bedrock "dolomite" in the study area. The observed value of Ca^{2+} versus Mg^{2+} ratio > 1 can increase the SAR, which can increase the salinity in these areas (Table 2). Based on the Wilcox plot of Na^+ versus EC (with a mean of 28 and range of 7.7–76) we can surmise that, with a few exceptional cases (with a high soluble sodium percentage (SSP), most of the CSR wells are excellent for irrigation. Some ESR wells with high EC (value up to 2910 µS/cm) were non-acceptable for irrigation practices (Fig. 6a). Kelley's ratio calculated for samples suggests that all samples of ESR (with a range of 0–0.5 and a mean of 0.5) and TSR (with a range of 0.5–1 and a mean of 0.7) with KR ≤ 1 are suitable, but fewer samples of CSR with a KR range of 0.1–3 with a mean of 0.6 shows that they are not suitable for crop irrigation in the region (Table 2). The potential salinity (PS) of the groundwater samples from the ESR site was between 0.8 and 12 (mean of 3.9). The calculated PS values at the CSR site had a mean of 3.7 (range 0.3–13.8) and the TSR site had a mean of 5.6 (range 1.8–8.3). The significantly higher PS value at all three Salt Range sites indicated that these wells were unsuitable for irrigation purposes (Doneen, 1964).

Higher Na^+ and SO_4^{2-} values could lead to a prolonged salinity (Batool et al., 2018). In the present study, the increasing sulfate trend in connection with high Na^+ concentrations in CSR and TSR shows a saltier environment. However, ECR showed a low salinity, except for the *Dalwal* (DLC) area, where the excessive extraction by the industrial facility

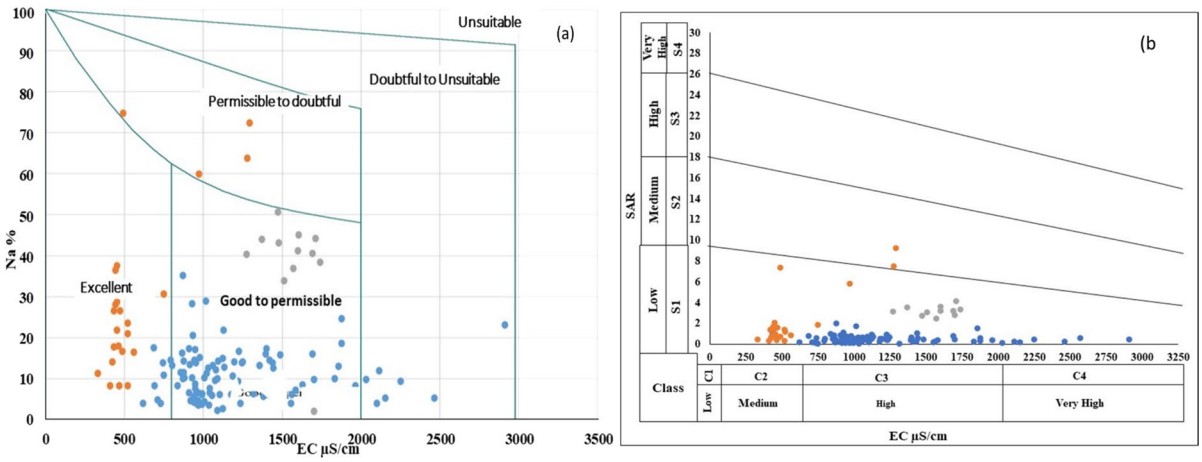

Fig. 6 **a** Suitability of irrigation water based on Wilcox diagram of Na% versus EC (Wilcox, 1955), **b** US salinity diagram for classification of irrigation waters after Richards on diagram (1954)

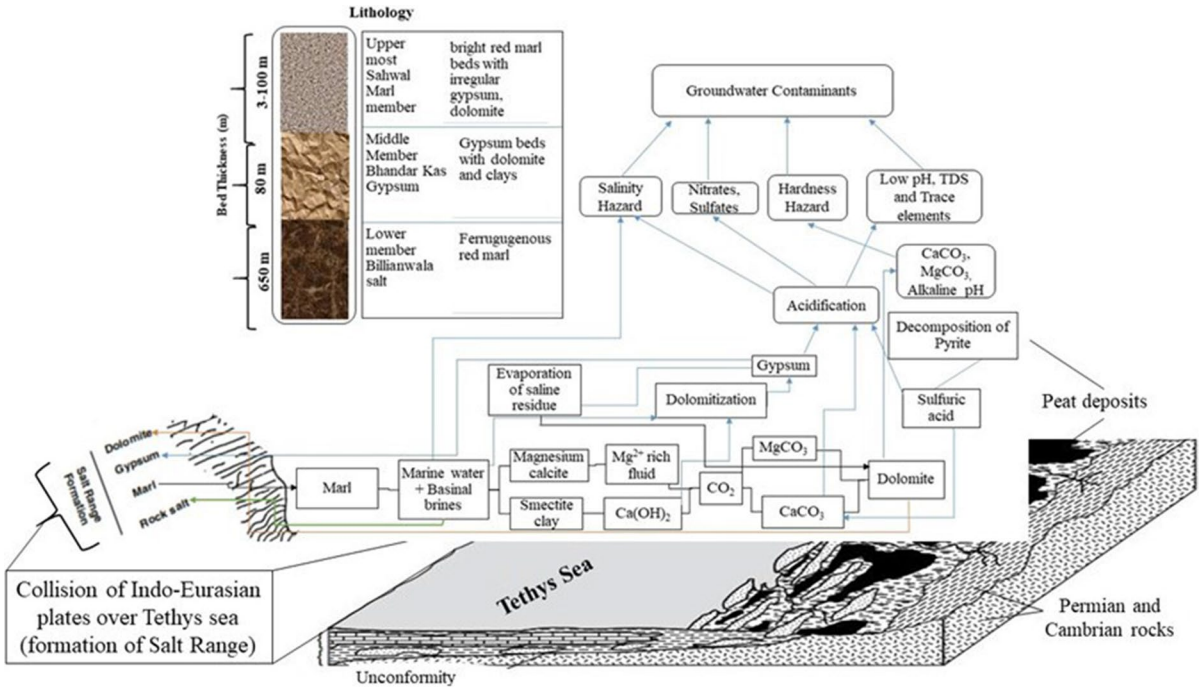

Fig. 7 Geochemical mechanisms defining water chemistry in coal bearing aquifers of Salt Range, Punjab

(cement-making unit on-site) increased the salinity of the deeper water through water–rock interaction. Overall, these results agree with the formation of salt water in the coal-based Munster land, Cretaceous Basin, Germany, where coal mining in the complex hydrogeological structure leads to a mixing of fluids and resultant highly saline groundwater in the area (Grobe and Machel, 2002) (Fig. 7).

Based on the complex geological formation and observed physico-chemical parameters, a conceptual model was developed to illustrate the main driving forces behind the water–rock interactions that define the water chemistry of the present study area (Fig. 7). The Salt Range underground stratigraphy is divided into three units (i.e., Sahwal marl member, Bhandar Kas gypsum, and Billianwala Salt member) (Fig. 7). It describes a closed basin with clastic and non-clastic evaporates and very dry climatic conditions. These Precambrian evaporite deposits formed by marine transgression and epicontinental sea led to dolostone forming (Butt & Mateen, 1996). In the Salt Range terrain, the hydrocarbon deposits of Punjab embrace the dominance of dolostone (80%) and sandstone (20%) (Wandrey et al., 2004). Dolomite is the preliminary stage of dolostone, which can form through various mechanisms with subsequent dolomitization. Dolomitization is a geological process in which Ca^{2+} ions in calcites are replaced by Mg^{2+} ions and dolomites are formed (Fig. 7). After deposition, these carbonate minerals undergo dolomitization in the Early Cambrian under the influence of climatic changes, which is followed by the dissolving of unaltered ooids in an Mg-rich fluid in the marine environment (Mehmood et al., 2018). It can be explained by the stoichiometric equation (Eq. 9).

$$2CaCO_3 + Mg^{2+} \leftrightarrow CaMg(CO_3)_2 + Ca^{2+} \quad (9)$$

The relatively higher solubility of calcites in dolomite rock means that it is washed out as $Ca–HCO_3$, which later precipitates out of the solution when the geochemical conditions change (Morrow et al., 2000). This dolomite acts as a source of increased Ca and Mg concentrations in the groundwater and, when replaced by Na ions, creates a permanent hardness via a reverse recharging process. Another reason for paleo-salinities in the Salt Range is the major precursor for acidification i.e., the presence of sulfide minerals could generate strong acids (Fig. 7). Coal mining activities occurring in the region through the

release and oxidation of pyrite minerals can increase the potential for acid-based weathering of geologically bound carbon, readily soluble salinity, and trace element pollution in the area (Ross et al., 2018). In addition, carbon sequestration through the weathering of the carbonates (rock units of salt formations that house coal seams) could also promote the salty fluid (Li et al., 2014; Obiadi et al., 2016) (Eq. 10).

$$CaCO_3 + H_2SO_4 \leftrightarrow Ca^{2+} + SO_4^{2-} + CO_2 + H_2O \quad (10)$$

Thus, from this scenario, it can be concluded that extensive coal mining activities in the Salt Range, apart from land disturbances, released the geologically sequestered pyrite and increased acidification. This acidification could consciously change the biogeochemical cycles of S, C, Ca^{2+}, and Mg^{2+} and in turn worsen the salinity dynamics (Ross et al., 2018).

Conclusions

The current study of groundwater quality for drinking and irrigation purposes has shown that the water is highly alkaline, except for CSR, where it is moderately acidic to neutral. The likely control mechanisms behind ionic hydrochemistry were the weathering of carbonate and silicate minerals (rock dominance) and the reverse ion exchange reaction, followed by evapotranspiration processes. Based on the conceptual model, these pore waters, which have been in contact with the rocks, when mixed with the liquids generated by hydrogeological processes, result in highly salinized groundwater in the region. The conjugative results of EC, TDS, salinity, and hardness indicated that the permanent hardness of the water makes it unsuitable for domestic and industrial use. In terms of suitability for irrigation, water wells observed for SAR, MAR, Na%, and Kelley's ratio indicated that all three locations (ESR, TSR, and CSR) had the potential to increase the risk of salinity in the longer term. Hence, there is an urgent need to establish water purification units to reduce water salinity and hardness. The trace element assessment showed that the neutralization capacity of parent geological formations buffers the acidic content and reduces the overall trace element accumulation. However, continuous mining without ecological and economic considerations can lead to water quality crises in the region. In addition, elevated levels of SO_4^{2-}, Cl^-, F^-, and NO_3^- should be considered as an early warning of plumes of pollutants, and their mechanisms of mobilization should be carefully studied to alleviate related human health concerns.

Acknowledgements This manuscript is part of the first author's Ph.D. Thesis. We are thankful to Higher Education Commission (HEC) Pakistan for funding under their International Research Support Initiative Program (IRSIP), Environmental Hydro geochemistry Laboratory, Department of Environmental Science, Quaid-i-Azam University, Islamabad, University of Leeds, UK, and the Environment & Sustainability Institute, University of Exeter, for technical assistance in performing laboratory analysis.

Author contributions NM (Environmental Geochemistry Laboratory, Department of Environmental Sciences, Faculty of Biological Sciences, Quaid-i-Azam University) has designed the study, collected data, performed the analytical part, drafted, and revised the manuscript. Dr. TZ (School of Earth and Space Sciences, Peking University) helped in revising the manuscript. Prof. KH-E (Professor in sustainable mining at Camborne School of Mines and Environment and Sustainability Institute, University of Exeter,) assisted in formal analysis and investigation for lab analysis. Dr. AF (Associate Professor in the Environmental Geochemistry Laboratory, Department of Environmental Sciences, Faculty of Biological Sciences, Quaid-i-Azam University) provides technical and financial assistance in developing the whole manuscript. She is the supervisor of the first author and helped her from conceptualizing to finalizing her research work.

Funding We thank the Higher Education Commission (HEC) Pakistan for funding under their International Research Support Initiative Program (IRSIP) for providing IRSIP fellowship to conduct lab analysis at the University of Leeds, UK, and the University of Exeter.

Availability of data and materials Supplementary data are provided along with the manuscript.

Declarations

Conflict of interest The author declares no competing/conflict of interest.

Ethical approval The material is the author's original work, which has not been published in any other journal.

Consent to participate Informed consent has been taken from the participants included in the study.

Consent to publish All authors have read and approved the final version of the article to submit for possible publication.

References

Arshad, S. M., Tariqa, S. M., Shahzada, M., Bakarb, M. Z. A., & Waqasa, M. (2015). Water characterisation of coal mining areas of Chakwal, Punjab, Pakistan. *Pakistan Journal of Scientific and Industrial Research Series a: Physical Sciences, 58*(1), 41e46.

Batool, A., Aziz, S., & Imad, S. (2018). Physico-chemical quality of drinking water and human health: A study of Salt Range Pakistan. *International Journal of Hydrology, 2*(6), 668–677.

Bosman, C. (2009). *The Hidden dragon: Nitrate pollution from open-pit mines–a case study from the Limpopo Province, South Africa,* Carin Bosman Sustainable Solutions, Pretoria, Gauteng, Republic of South Africa.

Bouteraa, O., Mebarki, A., Bouaicha, F., Nouaceur, Z., & Laignel, B. (2019). Groundwater quality assessment using multivariate analysis, geostatistical modeling, and water quality index (WQI): A case of study in the Boumerzoug-El Khroub valley of Northeast Algeria. *Acta Geochimica, 38*(6), 796–814.

Butt, K. A., & Mateen, A. (1996). Nilawahan rift; a permian event in Salt Range, Pakistan. *Geological Bulletin, University of Peshawar, 29*, 41–49.

Chen, Q., Jia, C., Wei, J., Dong, F., Yang, W., Hao, D., Jia, Z., & Ji, Y. (2020). Geochemical process of groundwater fluoride evolution along global coastal plains: Evidence from the comparison in seawater intrusion area and soil salinization area. *Chemical Geology, 552*, 119779.

Cheung, K., Klassen, P., Mayer, B., Goodarzi, F., & Aravena, R. (2010). Major ion and isotope geochemistry of fluids and gases from coalbed methane and shallow groundwater wells in Alberta, Canada. *Applied Geochemistry, 25*(1), 307–1329.

Dlamini, A. E., & Demlie, M. (2020). Integrated hydrogeological, hydrochemical and environmental isotope investigation of the area around the Kusile power station, Mpumalanga, South Africa. *Journal of African Earth Sciences, 172*, 103958.

Doneen, L. D. (1964).*Water quality for agriculture*. Department of Irrigation. university of California, California, 48.

Federation. (2005). *Standard methods for the examination of water and wastewater*. American Public Health Association (APHA): Washington, DC, USA, 21.

Finkelman, R. B., Dai, S., & French, D. (2019). The importance of minerals in coal as the hosts of chemical elements: A review. *International Journal of Coal Geology, 212*, 103251.

Freeze, R. A., & Cherry, J. A. (1979). *1979, Groundwater*. Prentice-Hall.

Ghazi, S., Sharif, S., Zafar, T., Riaz, M., Haider, R., & Hanif, T. (2020). Sedimentology and Stratigraphic evolution of the early eocene nammal formation, salt range, Pakistan. *Stratigraphy and Geological Correlation, 28*, 745–764.

Ghazi, S., & Mountney, N. P. (2011). Petrography and provenance of the early Permian Fluvial Warchha sandstone, Salt Range, Pakistan. *Sedimentary Geology, 233*(1–4), 88–110.

Gibbs, R. J. (1970). Mechanisms controlling world water chemistry. *Sciences, 170*(3962), 1088–1090.

Grobe, M., & Machel, H. G. (2002). Saline groundwater in the Münsterland Cretaceous basin, Germany: Clues to its origin and evolution. *Marine and Petroleum Geology, 19*(3), 307–322.

Guo, Q., Wang, Y., Ma, T., & Ma, R. (2007). Geochemical processes controlling the elevated fluoride concentrations in groundwaters of the Taiyuan basin, Northern China. *Journal of Geochemical Exploration, 93*(1), 1–12.

Hussain, S. A., Han, F.-Q., Han, W., Rodríguez, A., Han, J.-L., Han, J., Nian, X.-Q., Yi, L., Ma, Z., & Widory, D. (2019). Climate change impact on the evolution of the saline lakes of the Soan–Sakaser valley (central Salt Range; Pakistan): Evidences from hydrochemistry and water (δD, δ18O) and chlorine (δ37Cl) stable isotopes. *Water, 11*(5), 912.

Hussain, W., Abbas, S. Q., & Hussain, S. (2015). Structure Investigation, Economics and Stratigraphy of the Paleozoic, Mesozoic and Cenozoic sequence in the vicinity eastern and western side of the Salt Range, Punjab Pakistan. *Journal of Information Communication Technologies Robotic Applications, 6*(1), 95.

Hussain, Y., Ullah, S. F., Hussain, M. B., Aslam, A. Q., Akhter, G., Martinez-Carvajal, H., & Cárdenas-Soto, M. (2017). Modelling the vulnerability of groundwater to contamination in an unconfined alluvial aquifer in Pakistan. *Environmental Earth Sciences, 76*(2), 84.

Jabbar Khan, A., Akhter, G., Gabriel, H. F., & Shahid, M. (2020). Anthropogenic effects of coal mining on ecological resources of the central Indus basin, Pakistan. *International Journal of Environmental Research and Public Health, 17*(4), 1255.

Jain, S. K. (2012). Sustainable water management in India considering likely climate and other changes. *Current Science, 102*, 177–188.

Li, P., Wu, J., Tian, R., He, S., He, X., Xue, C., & Zhang, K. (2018). Geochemistry, hydraulic connectivity and quality appraisal of multilayered groundwater in the Hongdunzi coal mine, Northwest China. *Mine Water and the Environment, 37*(2), 222–237.

Li, X., Park, J. H., Edraki, M., & Baumgartl, T. (2014). Understanding the salinity issue of coal mine spoils in the context of salt cycle. *Environmental Geochemistry and Health, 36*(3), 453–465.

Long, J., & Luo, K. (2020). Elements in surface and well water from the central North China plain: Enrichment patterns, origins, and health risk assessment. *Environmental Pollution, 258*, 113725.

Mahmood, F. N., Barbour, L. S., Kennedy, C., & Hendry, M. J. (2017). Nitrate release from waste rock dumps in the Elk valley, British Columbia, Canada. *Science of the Total Environment, 605*, 915–928.

Malkani, M. S., & Mahmood, Z. (2017). Mineral resources of Pakistan: Provinces and basins wise. *Geological Survey of Pakistan, Memoir, 25*, 1–179.

Masood, N., Batool, S., & Farooqi, A. (2020). Groundwater pollution in Pakistan. In A. Mukherjee, B. R. Scanlon, & A. A. McKenzie (Eds.), *Global groundwater* (pp. 309–322). Elsevier.

Masood, N., Hudson-Edwards, K. A., & Farooqi, A. (2021). Groundwater nitrate and fluoride profiles, sources and

health risk assessment in the coal mining areas of Salt Range, Punjab Pakistan. *Environmental Geochemistry and Health, 44*, 15–728.

Masood, N., Zafar, T., Hudson-Edwards, K. A., Rehman, H. U., & Farooqi, A. (2022). Trace element geochemistry and stable isotopic (δ13C and δ15N) records of the Paleocene coals, Salt Range, Punjab, Pakistan. *International Journal of Mining Science and Technology*. https://doi.org/10.1016/j.ijmst.2022.03.007

Mazurek, I., Skawińska, A., & Sajdak, M. (2020). Analysis of chlorine forms in hard coal and the impact of leaching conditions on chlorine removal. *Journal of the Energy Institute*. https://doi.org/10.1016/j.joei.2020.10.002

Mehmood, M., Yaseen, M., Khan, E. U., & Khan, M. J. (2018). Dolomite and dolomitization model-a short review. *International Journal of Hydrology, 2*(5), 549–553.

Mohanty, A. K., Lingaswamy, M., Rao, V. V. S. G., & Sankaran, S. (2018). Impact of acid mine drainage and hydrogeochemical studies in a part of Rajrappa coal mining area of Ramgarh district, Jharkhand state of India. *Groundwater for Sustainable Development, 7*, 164–175.

Morrow, C. A., Moore, D. E., & Lockner, D. A. (2000). The effect of mineral bond strength and adsorbed water on fault gouge frictional strength. *Geophysical Research Letters, 27*(6), 815–818.

Negrel, P., Pauwels, H., Dewandel, B., Gandolfi, J. M., Mascré, C., & Ahmed, S. (2011). Understanding groundwater systems and their functioning through the study of stable water isotopes in a hard-rock aquifer (Maheshwaram watershed, India). *Journal of Hydrology, 397*(1–2), 55–70.

Nordstrom, D. K. (2008). *Questa baseline and pre-mining ground-water quality investigation 25. Summary of results and baseline and pre-mining ground-water geochemistry, Red River valley, Taos County, New Mexico, 2001–2005*. US Geological Survey.

Nordstrom, D. K., Blowes, D. W., & Ptacek, C. J. (2015). Hydrogeochemistry and microbiology of mine drainage: An update. *Applied Geochemistry, 57*, 3–16.

Obiadi, I. I., Obiadi, C. M., Akudinobi, B. E. B., Maduewesi, U. V., & Ezim, E. O. (2016). Effects of coal mining on the water resources in the communities hosting the Iva valley and Okpara coal mines in Enugu state, southeast Nigeria. *Sustainable Water Resources Management, 2*(3), 207–216.

Ochieng, E. G., Price, A. D. F., Egbu, C. O., Ruan, X., & Zuofa, T. (2015). Fresh driver for economic growth: Fracking the UK nation. *International Journal of Energy Sector Management*. https://doi.org/10.1108/IJESM-10-2014-0004

Okiongbo, K. S., & Akpofure, E. (2014). Identification of hydrogeochemical processes in groundwater using major ion chemistry: A case study of Yenagoa and environs, southern Nigeria. *Global Journal of Geological Sciences, 12*, 39–52.

Qurat-ul-Ain, Farooqi, A., Sultana, J., & Masood, N. (2017). Arsenic and fluoride co-contamination in shallow aquifers from agricultural suburbs and an industrial area of Punjab, Pakistan: Spatial trends, sources and human health implications. *Toxicology and Industrial Health, 33*(8), 655–672.

Raju, N. J., Shukla, U. K., & Ram, P. (2011). Hydrogeochemistry for the assessment of groundwater quality in Varanasi: A fast-urbanizing center in Uttar Pradesh, India. *Environmental Monitoring and Assessment, 173*(1–4), 279–300.

Reddy, K. J., Whitman, A. J., & Kniss, A. R. (2014). Potential beneficial uses of coalbed natural gas (CBNG) water. *Environmental Science Process Impact, 16*(1), 148–158.

Rehman, S., Shah, A. N., Mughal, H. U., Javed, M. T., Akram, M., Chilton, S., & Nimmo, W. (2016). Geology and combustion perspectives of Pakistani coals from Salt Range and trans indus range. *International Journal of Coal Geology, 168*, 202–213.

Richards, L. A. (1954). *Diagnosis and improvement of saline and alkali soils* (Vol. 78). LWW.

Ross, M. R. V., Nippgen, F., Hassett, B. A., McGlynn, B. L., & Bernhardt, E. S. (2018). Pyrite oxidation drives exceptionally high weathering rates and geologic CO_2 release in mountaintop-mined landscapes. *Global Biogeochemical Cycles, 32*(8), 1182–1194.

Sahoo, S., & Khaoash, S. (2020). Impact assessment of coal mining on groundwater chemistry and its quality from Brajrajnagar coal mining area using indexing models. *Journal of Geochemical Exploration, 215*, 106559.

Saou, A., Maza, M., & Seidel, J. L. (2012). Hydrogeochemical processes associated with double salinization of water in an algerian aquifer, carbonated and evaporitic. *Polish Journal of Environmental Studies, 21*(4), 1013–1024.

Shah, H. (2005). Livelihood assets and livelihood strategies of small farmers in Salt Range: A case study of Pind Dadan Khan District Jhelum, Pakistan. *Pakistan Journal of Agriculture Science, 42*(1–2), 82–88.

Shah, M. R., Abbasi, I. A., Haneef, M., & Khan, A. (1993). Nature, origin and mode of occurrence of Hangu-Kachai area coal, district Kohat, NWFP, Pakistan: A preliminary study. *Geological Bulletin, 26*, 87–94.

Singh, A. K., Mondal, G. C., Kumar, S., Singh, T. B., Tewary, B. K., & Sinha, A. (2008). Major ion chemistry, weathering processes and water quality assessment in upper catchment of Damodar River basin, India. *Environmental Geology, 54*(4), 745–758.

Singh, G., Rishi, M. S., Herojeet, R., Kaur, L., & Sharma, K. (2019). Evaluation of groundwater quality and human health risks from fluoride and nitrate in semi-arid region of northern India. *Environmental Geochemistry and Health, 42*, 1833–1862.

Singh, U. K., Ramanathan, A. L., & Subramanian, V. (2018). Groundwater chemistry and human health risk assessment in the mining region of East Singhbhum, Jharkhand, India. *Chemosphere, 204*, 501–513.

Tarki, M., Dassi, L., Hamed, Y., & Jedoui, Y. (2011). Geochemical and isotopic composition of groundwater in the complex terminal aquifer in southwestern Tunisia, with emphasis on the mixing by vertical leakage. *Environmental Earth Sciences, 64*(1), 85–95.

Tay, C. K., Kortatsi, B. K., Hayford, E., & Hodgson, I. O. (2014). Origin of major dissolved ions in groundwater within the Lower Pra Basin using groundwater geochemistry, source-rock deduction and stable isotopes of 2 H and 18 O. *Environmental Earth Sciences, 71*(12), 5079–5097.

Wandrey, C. J., Law, B. E., & Shah, H. A. (2004). *Sembar Goru/Ghazij composite total petroleum system, Indus and Sulaiman–Kirthar geologic provinces, Pakistan and India*. US Department of the Interior, US Geological Survey.

Warwick, P. D., & Wardlaw, B. R. (2007). *Regional studies of the Potwar plateau area, northern Pakistan*. Geological Survey (US).

Whiticar, M. J. (1999). Carbon and hydrogen isotope systematics of bacterial formation and oxidation of methane. *Chemical Geology, 161*, 291–314.

WHO. (2011). *Guidelines for drinking-water quality*. World Health Organization *216*, pp. 303–304).

Wilcox, L. V. (1955). *Classification and use of irrigation waters*. US Department of Agriculture.

Williams, J., Stubbs, T., & Milligan, A. (2012). *An analysis of coal seam gas production and natural resource management in Australia*. Australian Council of Environmental Deans and Directors.

Wright, I. A., Belmer, N., & Davies, P. J. (2017). Coal mine water pollution and ecological impairment of one of Australia's most 'protected'high conservation-value rivers. *Water, Air, Soil Pollution, 228*(3), 90.

Wu, W., Qu, S., Nel, W., & Ji, J. (2020). The impact of natural weathering and mining on heavy metal accumulation in the karst areas of the Pearl River Basin, China. *Science of the Total Environment, 734*, 139480.

Yadav, K., Raphi, M., & Jagadevan, S. (2020). Geochemical appraisal of fluoride contaminated groundwater in the vicinity of a coal mining region: Spatial variability and health risk assessment. *Geochemistry, 81*(1), 125684.

Zhang, Z., & Qin, Y. (2018). A preliminary investigation on water quality of coalbed natural gas produced water for beneficial uses: A case study in the Southern Qinshui Basin, North China. *Environmental Science and Pollution Research, 25*, 21589–21604.